Journal of The Electrochemical Society, **162** (6) A974-A981 (2015)
0013-4651/2015/162(6)/A974/8/$33.00 © The Electrochemical Society

Amorphous Ultrathin TiO_2 Atomic Layer Deposition Films on Carbon Nanotubes as Anodes for Lithium Ion Batteries

Ming Xie,[a] Xiang Sun,[b] Changgong Zhou,[c] Andrew S. Cavanagh,[a,*] Hongtao Sun,[b,] Tao Hu,[b] Gongkai Wang,[b] Jie Lian,[b] and Steven M. George[a,d,z]**

[a]*Department of Chemistry and Biochemistry, University of Colorado, Boulder, Colorado 80309, USA*
[b]*Department of Mechanical, Aerospace & Nuclear Engineering, Rensselaer Polytechnic Institute, Troy, New York 12180, USA*
[c]*Natural Science Department, Lawrence Technological University, Southfield, Michigan 48075, USA*
[d]*Department of Mechanical Engineering, University of Colorado, Boulder, Colorado 80309, USA*

Amorphous TiO_2 (a-TiO_2) thin films were conformally coated onto the surface of hydroxyl functionalized multi-walled carbon nanotubes (CNTs) using atomic layer deposition (ALD). The electrochemical characteristics of the a-TiO_2/CNT nanocomposites were then determined using cyclic voltammetry and galvanostatic charge/discharge curves. The ultrathin TiO_2 ALD films displayed high specific capacity and high rate capability. The specific capacities of the a-TiO_2/CNT nanocomposites after 50 and 100 TiO_2 ALD cycles at 100 mA/g were 220 mAh/g and 240 mAh/g, respectively. For CNTs coated with 100 TiO_2 ALD cycles, 88% of the capacity at 100 mA/g could be maintained at 1 A/g. When the voltage window for the a-TiO_2/CNT nanocomposites was extended down to 0.5 V versus Li/Li^+, the CNTs coated with 50 and 100 TiO_2 ALD cycles exhibited specific capacities at 100 mA/g of 275 mAh/g and 312 mAh/g, respectively. These high capacities are higher than the bulk theoretical values and are attributed to additional interfacial charge storage resulting from the high surface area of the a-TiO_2/CNT nanocomposites. Free-standing TiO_2-CNT electrodes were also fabricated and displayed excellent capacity and rate capability. These results demonstrate that TiO_2 ALD on high surface area CNT substrates can provide high power and high capacity anodes for lithium ion batteries.
 [DOI: 10.1149/2.0501506jes]

Manuscript submitted July 14, 2014; revised manuscript received February 23, 2015. Published March 10, 2015.

Lithium-ion batteries (LIBs) are one of the most promising energy storage technologies resulting from their high energy density and reasonable rate capability.[1,2] LIBs have received significant attention for applications in portable electronics. Additional improvements in energy density, lifetime stability and rate capability are needed for the further implementation of LIBs in electric vehicles. These improvements may be provided by new materials and novel architectures for LIBs.[3,4]

Ti-based anodes, including $Li_4Ti_5O_{12}$ (LTO) and various TiO_2 polymorphs, are potential alternative materials to conventional carbon-based anodes.[5–7] Compared with the theoretical specific capacity for graphite of 372 mAh/g, LTO has a lower theoretical specific capacity of 175 mAh/g and a negligible volume change of 0.2%.[7] In comparison to graphite anodes, the higher operating voltage of LTO prevents SEI formation.[8] This advantage ensures a good reversibility for LTO and safe performance during extended cycling.[8] On the other hand, the low electrical conductivity of $\sim 10^{-13}$ S/cm and the low Li diffusion coefficient of 10^{-9} to 10^{-13} cm^2/s are major limitations for the LTO anode.[7]

TiO_2 polymorphs, including anatase, rutile, and TiO_2(B), have also been extensively studied as anodes for LIBs.[9–16] TiO_2 delivers a high discharge voltage plateau of ~1.7 V versus Li/Li^+ and has a small volume expansion of ~4% during lithiation/delithiation.[17,18] Anatase and rutile TiO_2 have a theoretical intercalation limit of 0.5 Li per TiO_2 or 168 mAh/g.[19] TiO_2(B) is expected to accommodate more lithium than any other TiO_2 polymorph with a theoretical capacity of ~335 mAh/g.[20–22] However, like LTO, Li^+ has slow bulk diffusion in TiO_2. The Li^+ ion diffusion coefficient in anatase TiO_2 is $\sim 10^{-13}$-10^{-17} cm^2/s.[23] The electrical conductivity of anatase is also low at $\sim 10^{-12}$ S/cm.[24] The low diffusivity and conductivity limit the rate for Li^+ insertion and extraction from the host TiO_2 lattice.

The problems with LTO and TiO_2 can be addressed by depositing ultrathin TiO_2 films on high surface area and high electrical conductance carbon substrates.[15,25–27] The TiO_2 films can be deposited using atomic layer deposition (ALD) techniques. ALD is based on sequential self-limiting reactions and provides precise control of film uniformity, thickness, composition and morphology.[28] ALD can deposit thin films on high aspect ratio substrates.[29,30] ALD also yields strong chemical bonding between the substrate and the deposited film that can enhance the cycle stability of the film during energy storage applications.

ALD has recently been successfully used to deposit metal oxides on carbon substrates for a variety of electrochemical applications. Al_2O_3 ALD films can enhance the capacity stability of carbon anodes in LIBs.[31,32] Various metal oxide ALD coatings, such as TiO_2, V_2O_5 and SnO_2, can also serve as active Li^+ storage materials on carbon supports for LIBs.[33–35] V_2O_5 and TiO_2 films on carbon substrates can also serve to increase charge storage for supercapacitor applications.[36–38] ALD has also been employed to deposit metal oxides on non-carbon substrates for Li ion microbattery applications. Examples include TiO_2 ALD on nickel or aluminum nanorods,[39,40] V_2O_5 ALD on nickel-coated virus nanostructures,[41] and TiO_2 ALD on silicon microtubes.[42]

In this work, we deposit ultra-thin amorphous TiO_2 (a-TiO_2) films on CNTs using ALD. Compared with crystalline TiO_2, nanoscale a-TiO_2 possesses a higher ion diffusion rate[43] as well as a higher capacity.[44] Recently, a-TiO_2 has received substantial attention as an anode for LIBs.[26,33,43–47] The amorphous morphology can help alleviate the volume change of ~4% during insertion/extraction that can be detrimental to charge/discharge cycling at high rates. However, unlike its polymorph counterparts, a-TiO_2 typically suffers large irreversible capacity loss on its first charge/discharge cycle.[24]

An illustration of ultrathin TiO_2 ALD films on CNTs is displayed in Figure 1. This nanocomposite electrode has many advantages. Ultrathin film thicknesses can greatly shorten both the Li^+ ion diffusion length and electron transfer path to assure exceptional rate capability for the a-TiO_2/CNT nanocomposite. In addition, the large surface area and excellent electrical conductivity of CNTs allow them to act as ideal hosts for promoting efficient electron transport between a-TiO_2 and the current collector. With ultrathin a-TiO_2 films on CNTs, improvements in the capacity of a-TiO_2 may be possible with excellent rate capacity and cyclability.

Experimental

ALD for a-TiO_2/CNT nanocomposites.— TiO_2 ALD on pristine CNTs will have initial nucleation difficulties due to the lack of reactive sites as reported previously.[48] TiO_2 ALD is expected to nucleate and grow only at defects and step edges on CNTs in the absence of an adhesion layer. Growth at these defects will result in a distribution of TiO_2 nanoparticles.[48] Earlier work on TiO_2 ALD on graphene obtained

*Electrochemical Society Active Member.
**Electrochemical Society Student Member.
zE-mail: steven.george@colorado.edu

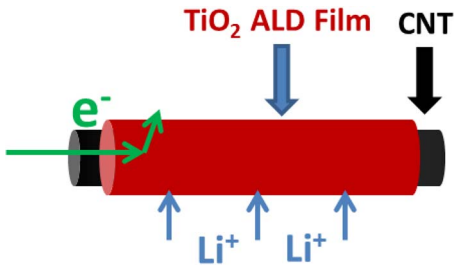

Figure 1. Schematic of TiO_2 ALD film on CNT. This architecture provides electron transport through CNT and facile Li^+ transport through ultrathin TiO_2 ALD film.

only anatase TiO_2 nanoparticles in the absence of an adhesion layer.[38] In contrast, continuous and amorphous TiO_2 ALD films were observed using an Al_2O_3 ALD adhesion layer.[37]

This work utilized hydroxyl (–OH) terminated CNTs. The hydroxyl functional groups served as the initial nucleation sites for reaction with the $TiCl_4$ ALD precursors. The surface chemistry for depositing a-TiO_2 on hydroxylated (–OH) functionalized CNT is shown in Figure 2. Because of the high concentration of –OH groups on the CNT surface and low deposition temperature of 120°C, the deposited TiO_2 is expected to grow as a continuous amorphous film.[49]

TiO_2 ALD films were grown on CNT powders using a rotary ALD reactor.[48,50,51] The CNT powders are composed of entangled aggregates of CNTs.[48] The rotary reactor agitates the powders during ALD and prevents particle aggregation. Hydroxyl terminated multiwalled CNTs were purchased from Nanostructured & Amorphous Materials, Inc. TiO_2 ALD was deposited utilizing titanium tetrachloride ($TiCl_4$) and H_2O as the precursors at 120°C according to the following surface reactions:[52]

$$(A)\ TiOH^* + TiCl_4 \rightarrow TiO\text{-}TiCl_3^* + HCl \quad [1]$$

$$(B)\ TiCl^* + H_2O \rightarrow Ti\text{-}OH^* + HCl \quad [2]$$

The performance of both of these A and B reactions constitutes one TiO_2 ALD cycle. $TiCl_4$ (99.8%, Strem Chemicals) and high performance liquid chromatography (HPLC) grade H_2O (Sigma-Aldrich) were utilized for the TiO_2 ALD.

The TiO_2 ALD reactions were performed using static exposures in the rotary ALD reactor. The reaction sequence was: i) dose $TiCl_4$ to 1.0 Torr for 120 seconds; ii) evacuate the reaction products and excess $TiCl_4$; iii) dose N_2 to 20.0 Torr for 60 seconds and then evacuate N_2 (repeat 5 times); iv) dose H_2O to 1.0 Torr for 120 seconds; v) evacuate the reaction products and excess H_2O; vi) dose N_2 to 20.0 Torr for 60 seconds and then evacuate N_2 (repeat 5 times). Using this reaction sequence, the TiO_2 film thickness was precisely controlled by the number of TiO_2 ALD reaction cycles.

Structure characterization and electrochemical testing.— X-ray diffraction (XRD) measurements were performed using a PANanalytical X-ray diffraction system. Thermogravimetric analysis (TGA) was performed in air from 30°C to 800°C at a heating rate of 10°C/min using a TA Instruments TGA-Q50. Transmission electron microscopic images were obtained using a JEOL JEM-2010 with an operating voltage at 200 kV. X-ray photoelectron spectroscopy (XPS) was performed using a PHI 5000 Versa Probe system.

The electrodes were made by mixing the a-TiO_2/CNT nanocomposites with polyvinylidene fluoride and carbon black with a weight ratio of 80:10:10 in 1-methyl-2-pyrrolidinone solvent. The slurry was spread by doctor blading on copper foil and dried in vacuum at 80°C. All of the cells were then assembled in an argon-filled dry box with Li metal as the counter electrode.

A Celgard separator 2340 and 1 M $LiPF_6$ electrolyte solution in ethylene carbonate: diethyl carbonate (Novolyte) (1:1 by mass) were used to fabricate the coin cells. Cyclic voltammetry was performed with a potentiostat VersaSTAT 4 from Princeton Applied Research. The galvanostatic charge/discharge characteristics were analyzed using an Arbin BT-2143 Battery Station. The electrode mass loading was ~2 mg/cm^2.

Fabrication of free-standing TiO_2-CNT paper.— The freestanding electrode consisted of a-TiO_2/CNT nanocomposites grown using 100 TiO_2 ALD cycles. These a-TiO_2/CNT nanocomposites also contained 10% uncoated CNTs by mass. Free-standing electrodes were fabricated using a filtration method with a proprietary solvent developed by Buckeye Composites. Briefly, 90% TiO_2-CNT nanocomposites and 10% pristine CNT powders by mass were dispersed in the solvent without surfactants. The diameter of the filter paper was 47 mm. The areal TiO_2 mass loading was 5 mg/cm^2.

Results and Discussion

TiO_2 ALD on CNTs.— Figure 3 displays the XRD patterns of the TiO_2-CNT nanocomposites grown using 50 and 100 TiO_2 ALD cycles at 120°C. The TiO_2-CNT nanocomposites grown using 50 and 100 TiO_2 ALD cycles are designated as TiO_2-CNT-1 and TiO_2-CNT-2, respectively. The CNT-containing samples exhibited a strong (002) peak at 26° attributed to the structure of the CNT.[53] The much weaker peaks at ~44° and ~54° are also derived from the CNTs.[53,54] No peaks were identified that could be assigned to the anatase or rutile crystalline phases of TiO_2. The absence of these peaks is consistent with amorphous TiO_2. TiO_2 ALD forms an amorphous film at 100–140°C.[49] The anatase TiO_2 phase can be formed with deposition temperatures

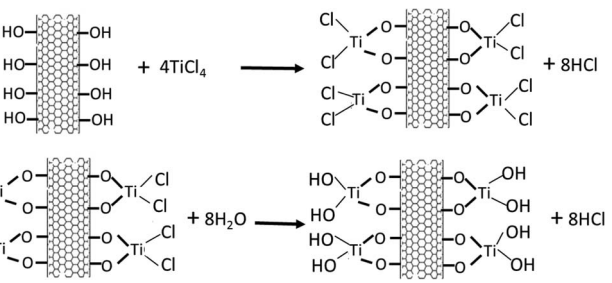

Figure 2. Schematic of surface chemistry of TiO_2 ALD using $TiCl_4$ and H_2O on hydroxyl-functionalized CNT.

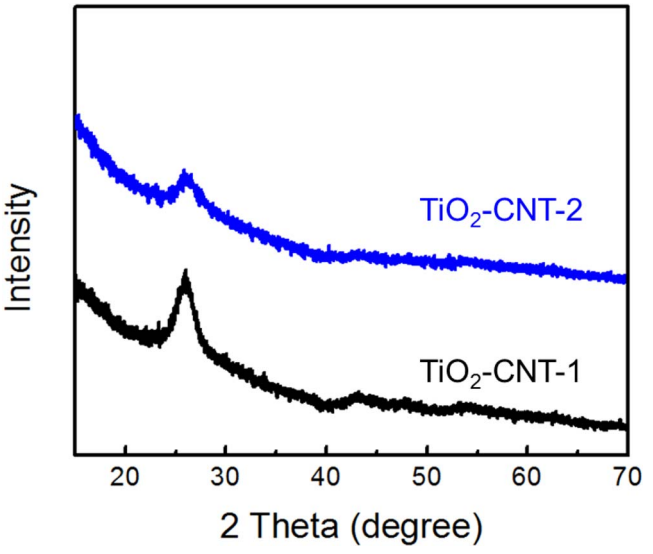

Figure 3. XRD scans of TiO_2-CNT samples fabricated using 50 and 100 TiO_2 ALD cycles. These samples are designated TiO_2-CNT-1 and TiO_2-CNT-2, respectively.

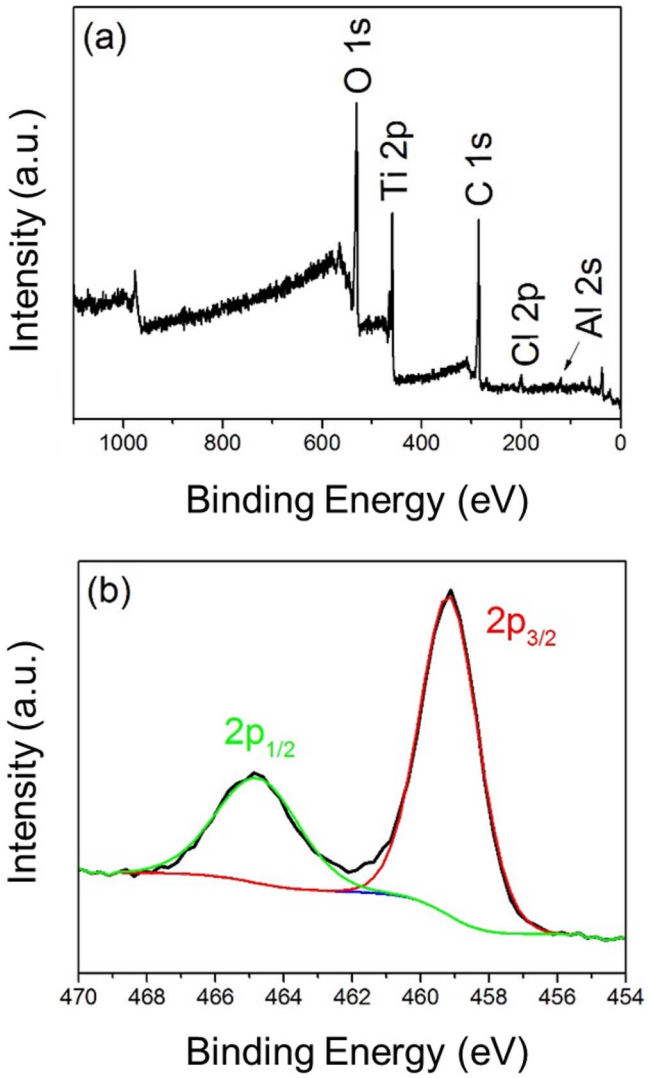

Figure 4. XPS spectra for TiO_2-CNT-2 after 100 TiO_2 ALD cycles on the CNT samples. (a) XPS survey spectrum and (b) Ti2p region of XPS spectrum.

>160°C.[49] The a-TiO_2 films grown on the hydroxyl functionalized CNTs are important because a-TiO_2 may exhibit higher charge storage capability than crystalline phases.[33,43–46]

The presence of TiO_2 on the surface of the CNTs was confirmed by X-ray photoelectron spectroscopy (XPS). As shown in Figure 4a, the TiO_2/CNT nanocomposites exhibited characteristic XPS peaks for titanium, oxygen, carbon and chlorine. The small amount of chlorine shown in the survey XPS scan in Figure 4a is from incomplete surface reactions during the TiO_2 ALD growth process.[52] Figure 4b shows the spectra of Ti 2p peaks located at 464.9 and 459.2 eV with a peak separation of 5.7 eV. These peak locations and separation are in excellent agreement with the reported values for TiO_2.[55–57] These XPS results verify the presence of TiO_2 on the CNTs.

The film thickness and morphology of the TiO_2 ALD on the edges of hydroxyl functionalized CNTs were further investigated by transmission electron microscopy (TEM). Figure 5 shows that the edges of the CNTs are conformally coated by the TiO_2 ALD films. The typical TiO_2 growth rate by ALD is ~0.6 Å/cycle.[52] As shown in Figure 5a and 5b, TiO_2 ALD film thicknesses of ~3 nm and ~12 nm were obtained after 50 and 100 TiO_2 ALD cycles, respectively. The slightly larger TiO_2 ALD film thicknesses after 100 TiO_2 ALD cycles could result from some additional TiO_2 chemical vapor deposition resulting from incomplete H_2O purging as the TiO_2 ALD films build up on the CNTs.

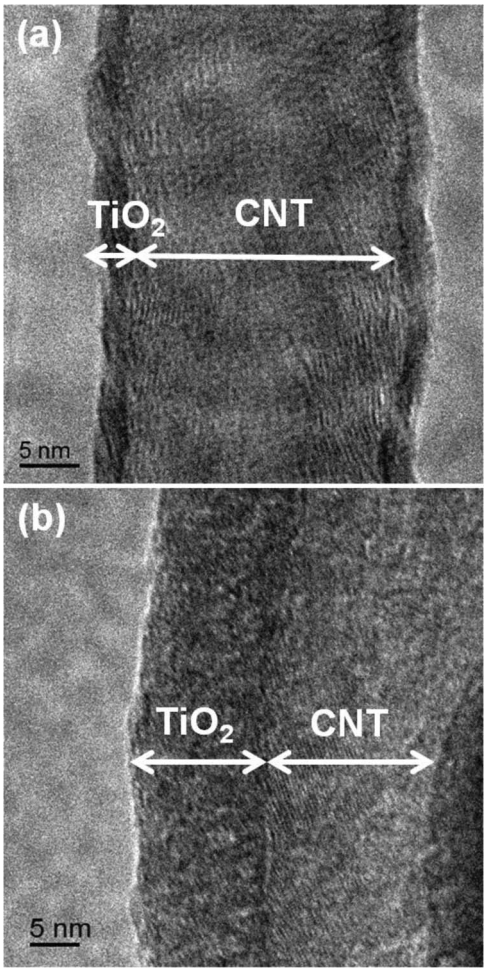

Figure 5. TEM image of edge of CNT for (a) TiO_2-CNT-1 after 50 cycles of TiO_2 ALD and (b) TiO_2-CNT-2 after 100 cycles of TiO_2 ALD.

Figure 6 shows the film thickness and morphology of the TiO_2 ALD film on the end of a hydroxyl functionalized CNT. This TEM image was obtained after 100 TiO_2 ALD cycles. The TiO_2 ALD film has a thickness of ~12 nm and is conformal on the edge of the CNT. The TiO_2 ALD film has the same thickness of ~12 nm and remains conformal around the end of the CNT. This conformal and equivalent

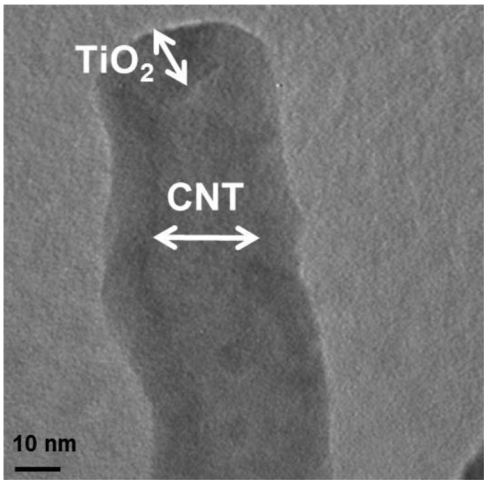

Figure 6. TEM image of end of CNT for TiO_2-CNT-2 after 100 cycles of TiO_2 ALD.

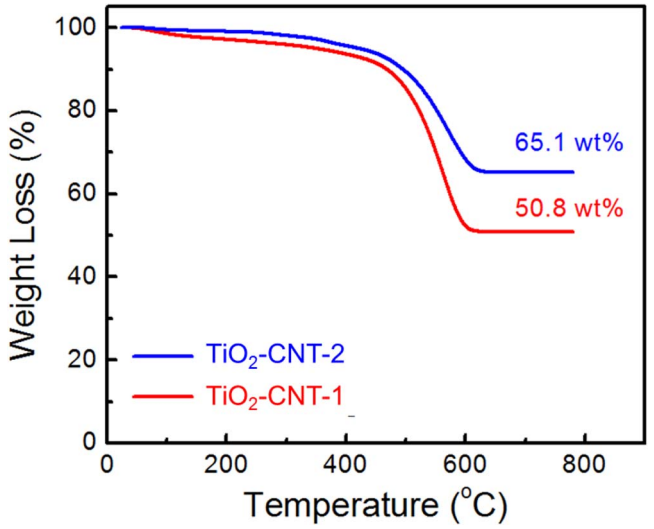

Figure 7. TGA results for TiO_2-CNT-1 and TiO_2-CNT-2 after 50 and 100 TiO_2 ALD cycles, respectively.

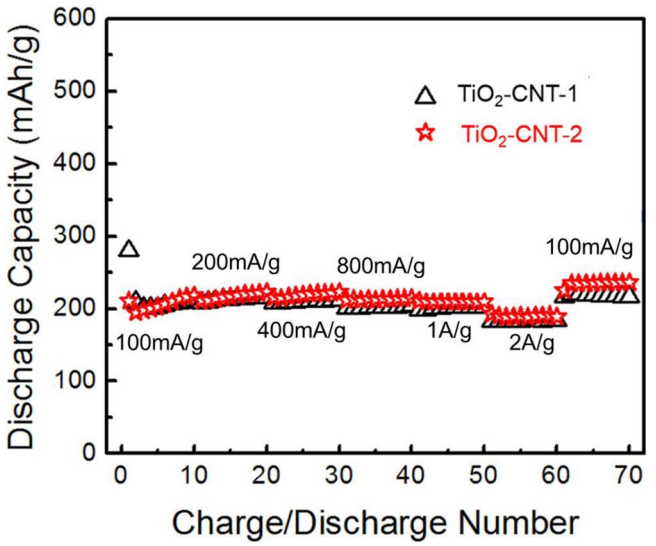

Figure 8. Rate performance of TiO_2-CNT-1 and TiO_2-CNT-2 using a voltage window of 1.0-3.0 V versus Li/Li^+.

TiO_2 ALD film thickness indicates that TiO_2 ALD is able to nucleate readily on both the edge and end of the hydroxyl functionalized CNT.

The weight percentage of TiO_2 in the composites was determined by thermal gravimetric analysis (TGA) assuming that the CNTs are completely oxidized after reaching 600°C. The TGA results are displayed in Figure 7. TiO_2 mass percentages of 50.8% and 65.1% were obtained for TiO_2-CNT-1 and TiO_2-CNT-2, respectively. These high mass loadings of TiO_2 on the CNTs are important for the successful implementation of ALD to deposit active materials on conductive substrates to fabricate electrodes for Li^+ ion batteries.

This work employed static dosing of the ALD precursors in the rotary ALD reactor instead of flow-type dosing. Static dosing can reach much higher reactant utilization and facilitates more conformal deposition on high surface area substrates.[29,51] One drawback of employing ALD for large scale production is the time required to deposit the ALD coatings. This drawback can be overcome by implementing ALD on high surface area substrates where >50 wt% active material can be deposited with 50–100 ALD cycles. At this time, our rotary ALD reactor has the capability of forming ALD nanocomposites with initial batch quantities of 10 g of CNT powder per ALD coating run.

Electrochemical testing.— Coin cells were used to evaluate the electrochemical performance of a-TiO_2/CNT as anode materials. Excellent rate performance has been achieved using a-TiO_2/CNT nanocomposites fabricated using 50 and 100 ALD cycles. Figure 8 shows the rate performance at various current densities in the voltage range of 1.0–3.0 V versus Li/Li^+. The cell has been continuously cycled without any rest between the different charge/discharge rates. The results for TiO_2-CNT-1 and TiO_2-CNT-2 are very similar at the different charge/discharge rates. Figure 9 displays the voltage versus capacity during lithiation and delithiation for the 1st and 10th charge/discharge cycles at 100 mA/g shown in Figure 8.

At a rate of 100 mA/g, Figure 8 shows that TiO_2-CNT-1 and TiO_2-CNT-2 exhibit discharge capacities of 220 and 240 mAh/g, respectively, after 60 total charge/discharge cycles. These discharge capacities are slightly higher than the discharge capacities at 100 mA/g during the first 10 charge/discharge cycles because of activation processes in the electrode. These capacities are higher than the capacities measured earlier for a-TiO_2 on graphene.[33] These capacities are also significantly higher than the theoretical capacities of 168 mAh/g and 175 mAh/g for anatase TiO_2 and $Li_4Ti_5O_{12}$. When the current rate is increased to 1 A/g, the a-TiO_2/CNT nanocomposite still maintains about 88% of its capacity at 100 mA/g. These results demonstrate the exceptional rate capability of these samples.

The almost identical capacities for TiO_2-CNT-1 and TiO_2-CNT-2 indicate that the TiO_2 coatings are thin enough that bulk diffusion is not limited by the thickness of TiO_2 film. When the current density is further increased to 10 A/g in Figure 10a, TiO_2-CNT-2 still exhibits a capacity of 120 mAh/g. After 1000 charge/discharge cycles at 10 A/g, Figure 10b shows that TiO_2-CNT-2 still maintains 95% of its initial capacity. To the best of our knowledge, this a-TiO_2/CNT nanocomposite displays the highest specific capacity at the highest rate and exhibits the highest rate retention compared with all other TiO_2 anodes. A compilation of the previous results for the highest performance TiO_2 anodes is given in Table I.

The Coulombic efficiency in the first charge/discharge cycle is crucial for LIBs. Low Coulombic efficiency will consume Li^+ ions provided by the cathode and result in a rapid capacity fading. TiO_2 has a better initial Coulombic efficiency compared with graphite anodes. However, some irreversible loss in the first several charge/discharge cycles is still observed for TiO_2. Although the cutoff voltage of 1.0 V versus Li/Li^+ for the TiO_2 anode is higher than voltage of ~0.8 V for SEI formation, some irreversible reactions may still contribute to this loss.[9]

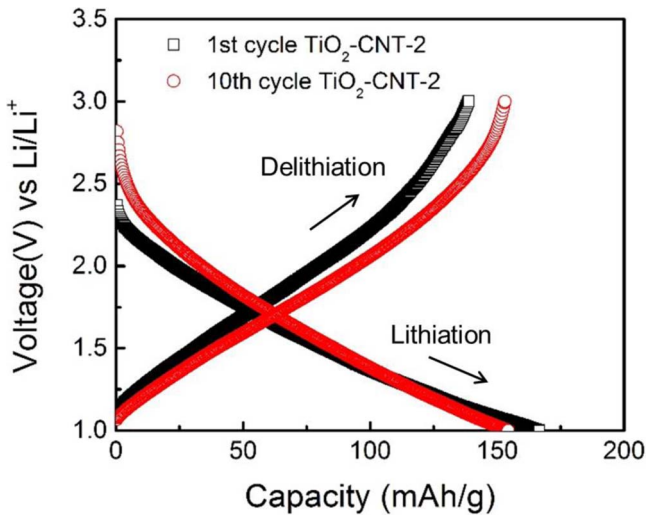

Figure 9. Voltage versus capacity during lithiation and delithiation for the 1st and 10th charge/discharge cycles at 100 mA/g shown in Figure 8.

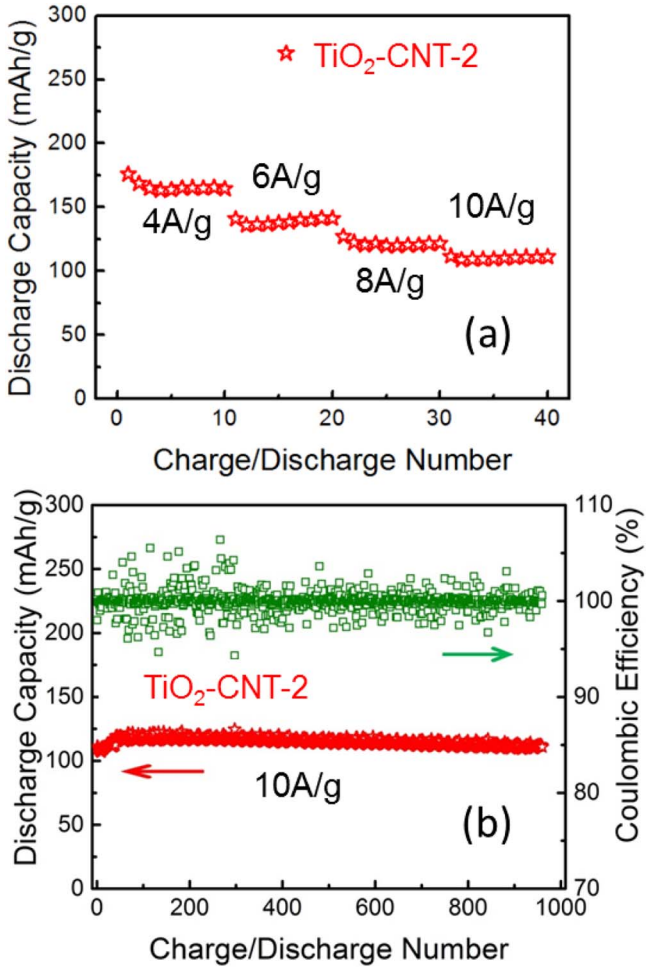

Figure 10. (a) Rate performance of TiO_2-CNT-2 and (b) capacity retention and Coulombic efficiency of TiO_2-CNT-2 at 10A/g for 1000 charge/discharge cycles using a voltage window of 1.0–3.0 V versus Li/Li^+.

In this work, TiO_2-CNT-2 displayed an initial Coulombic efficiency during the first charge/discharge cycle of 83.3%. In comparison, TiO_2-CNT-1 yielded an initial Coulombic efficiency during the first charge/discharge cycle of 70.4%. This initial Coulombic efficiency was measured prior to recording the discharge capacities shown in Figure 10b. The efficiency loss is attributed to irreversible loss of surface area from the CNT matrix. In comparison, CNTs usually show a higher irreversible loss with Coulombic efficiency for the first charge/discharge cycle of only <50%.[58]

The solid electrolyte interphase (SEI) can be formed particularly at defects and edge planes of carbonaceous anodes.[59] For example, the oxygen-containing surface functional groups on graphene are very reactive and can oxidize the electrolyte and induce electrochemical instability of the electrode.[60,61] Al_2O_3 ALD can help improve the Coulumbic efficiency and capacity retention of natural graphite and CNTs.[31,32] Like Al_2O_3 ALD, TiO_2 ALD may both provide an active anode material and also serve as a protective layer on the CNTs to reduce SEI formation and irreversible loss. After the first cycle, Figure 10b shows that TiO_2-CNT-2 displays Coulumbic efficiencies close to 100%.

TiO_2 and LTO can provide exceptional rate capability and lifetime. However, their operating potential between 1.0–3.0 V versus Li/Li^+ and their inherent structure lead to a low energy density relative to graphite. In contrast, carbon-based anodes are not suitable for high-power application because of their low intercalation potential of <0.1 V versus Li/Li^+. This low potential causes lithium plating and dendrite growth during fast charge/discharge rate.[62,63]

To improve the energy density, TiO_2 can be operated in an enlarged potential window. Several studies have previously explored enlarged potential windows.[14,64,65] All of these studies used voltages as low as 0.01 V versus Li/Li^+ to extract the most capacity. Unfortunately, this low voltage will lead to lithium dendrite growth at high rate and cause safety concerns. Therefore, a cutoff voltage of 0.5 V versus Li/Li^+ was utilized in this study to achieve a balance between energy density and safety.

Cyclic voltammograms (CV) of TiO_2/CNT nanocomposites were measured between 0.5 and 3.0 V versus Li/Li^+ at a scan rate of 0.05 mV/s. The CV scan at 5 mV/s for TiO_2-CNT-2 is displayed in Figure 11. European convention is employed where voltage is more positive with scanning to the right and the anodic current is positive. The anodic current is expected to result from lithium extraction from TiO_2. However, there may also be anodic current from Li^+ ions being released from the electric double layer or Li^+ ions leaving the TiO_2 surface as a result of faradaic processes. The cathodic current is expected to result from lithium insertion in TiO_2. However, there may also be cathodic current from Li^+ ions charging the electric double layer or Li^+ ions being stored at the interface resulting from faradaic processes.

In the voltage range of 0.5–3.0 V versus Li/Li^+, the first cycle shows a large irreversible cathodic current peak starting at ~0.8 eV, that is attributed to SEI formation on the surface.[66] After the 3rd cycle, TiO_2-CNT-2 shows very reversible behavior. Both the anodic and cathodic current densities versus potential are nearly featureless. No anodic or cathodic peaks are observed between 1.5–2.0 V versus Li/Li^+ that are commonly observed for crystalline TiO_2.[8,9,11,14,16] The fairly constant current density versus potential is consistent with amorphous TiO_2.[43,45,46] The current density versus potential in Figure 11 is very similar to the current density versus potential observed in Figure 7 of Reference 46 for high surface area amorphous TiO_2 films prepared using ballistic deposition methods.[46]

Table I. Performance of TiO_2 Anode Materials.

Morphology & Crystallinity	Highest Capacity (1.0–3.0V)	Capacity Retention	Capacity at High Rate	Reference
Nanoporous anatase TiO_2	250 mAh/g at C/5	62% from 1C to 10C	46 mAh/g at 60C	9
Ultrathin TiO_2 nanosheets	200 mAh/g at 2C	75% from 2C to 20C	100 mAh/g at 50C	10
Mesoporous anatase TiO_2 Nanospheres	200 mAh/g at 1C	80% from 1C to 10C	100 mAh/g at 50C	11
Nitridated TiO_2 nanofibers	160 mAh/g at C/5	25% from 1C to 10C	30 mAh/g at 10C	12
Hydrogen reduced TiO_2 nanoparticles	180 mAh/g at C/5	71.4% from 1C to 10C	130 mAh/g at 10C	13
TiO_2 Nanocages	150 mAh/g at C/2	76.9% from 1C to 10C	100 mAh/g at 10C	14
Graphene-based TiO_2 nanosheets	200 mAh/g at C/5	75% from 1C to 10C	90 mAh/g at 50C	15
Porous TiO_2-B nanosheet	225 mAh/g at C/5	88.8% from 1C to 10C	160 mAh/g at 30C	16
Amorphous TiO_2-CNT nanocomposites	240 mAh/g at C/1.7 220 mAh/g at 1.18C 312 mAh/g at C/1.7 (0.5–3.0V)	88.8% from 1.2C to 12C	120 mAh/g at 59C	This work

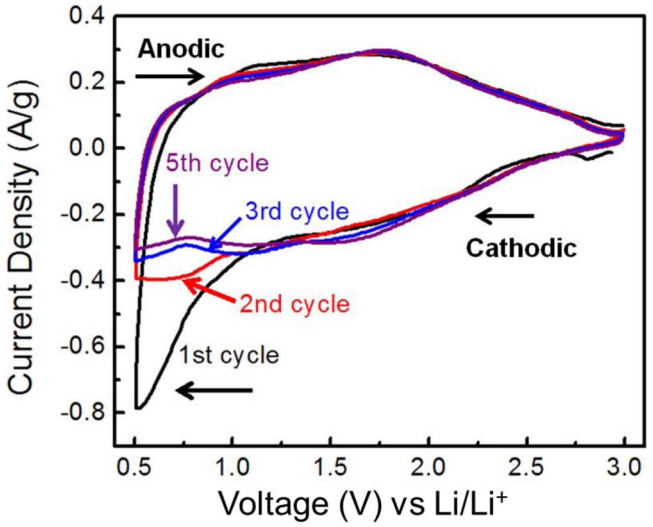

Figure 11. Cyclic voltammetry (CV) at 5 mV/s of TiO_2-CNT-2 using an extended voltage window of 0.5–3.0 V versus Li/Li^+.

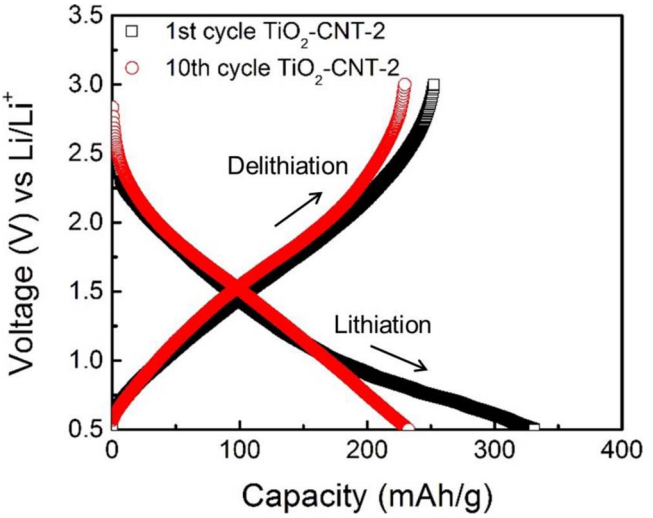

Figure 13. Voltage versus capacity during lithiation and delithiation for the 1st and 10th charge/discharge cycles at 100 mA/g shown in Figure 12.

Amorphous TiO_2 displays more "box-like" current versus voltage that is suggestive of capacitive behavior. The CV results displayed in Figure 11 are more "box-like" and capacitive than the previous pseudocapacitance results for anatase TiO_2 nanoparticles or continuous amorphous TiO_2 films on graphene or CNTs using an Al_2O_3 ALD adhesion layer.[37,38] These earlier CV results for TiO_2 employed as a supercapacitor were obtained using a 1 M KOH electrolyte.

Figure 12 shows the rate performance at various current densities in the extended voltage range between 0.5–3.0 V versus Li/Li^+ for TiO_2-CNT-1 and TiO_2-CNT-2. Figure 13 displays the voltage versus capacity during lithiation and delithiation for the 1st and 10th charge/discharge cycles at 100 mA/g shown in Figure 12. The specific capacity of a-TiO_2 was calculated by subtracting the CNT contributions from the nanocomposites. The discharge capacity of the CNTs by themselves was small relative to the TiO_2 ALD-coated CNT samples. The discharge capacities of the uncoated CNTs were ~35 mAh/g at 100 mA/g and decreased to ~5 mAh/g at 2 A/g. The actual contribution of the CNTs in the evaluation of the TiO_2 ALD-coated CNT electrodes could have been even lower because the CNTs are completely covered with TiO_2 ALD films.

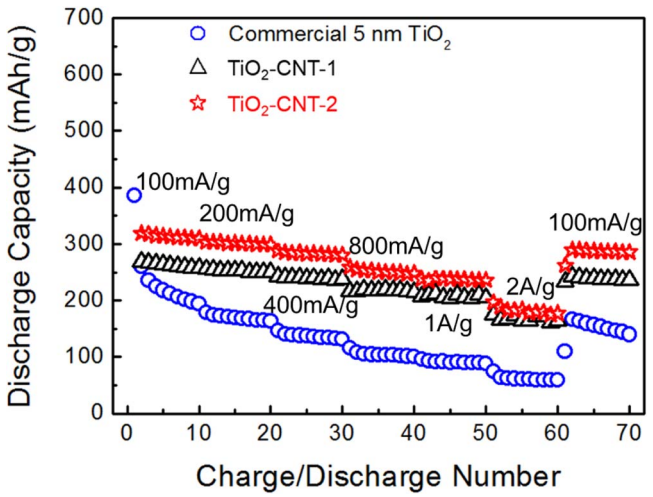

Figure 12. Rate performance of TiO_2-CNT-1 and TiO_2-CNT-2 using an extended voltage window of 0.5–3.0 V versus Li/Li^+. The rate performance of commercial 5 nm TiO_2 particles is shown for comparison.

At a rate of 100 mA/g, TiO_2-CNT-1 and TiO_2-CNT-2 exhibited discharge capacities of 275 mAh/g and 312 mAh/g for 0.5–3.0 V, respectively, compared with 220 and 240 mAh/g for 1.0–3.0 V, respectively. The difference between the specific capacities for TiO_2-CNT-1 and TiO_2-CNT-2 is larger than the experimental error of <5%. The capacity of 312 mAh/g corresponds to a stoichiometry of $Li_{0.93}TiO_2$. This capacity is much higher than the theoretical capacity for $Li_{0.5}TiO_2$ of 167 mAh/g. This capacity is the highest value ever reported for TiO_2 and LTO anodes even when including the previous work with potentials as low as 0.1 V versus Li/Li^+. This capacity would be even higher if the contribution from the CNTs to the capacity is less than the uncoated CNTs by themselves.

Large capacities that are higher than theoretical predictions have been previously attributed to interfacial charge storage phenomena.[9,23,67–69] A similar explanation can be employed to explain the high capacity with excellent rate capacity in the current study on amorphous TiO_2 ALD films on CNTs. The "box-like" appearance of the cathodic and anodic current densities after the 3rd charge/discharge cycle is also consistent with capacitive interfacial charge storage behavior.[70,71] Charge storage in the electric double layer and on the TiO_2 surface via faradaic reactions can provide much higher capacities than the capacities in the TiO_2 bulk alone.

Support for interfacial charge storage is provided by the high discharge capacities even at high discharge rates that are shown in Figure 12. When the current rate is increased to 1 A/g, TiO_2-CNT-2 still preserves about 79% of the capacity observed at 100 mA/g. This capacity retention is higher than most of the previous TiO_2/carbon composites listed in Table I. For the more restrictive potential cycling from 1.0–3.0 V versus Li/Li^+, an even higher rate retention of 88.8% is observed when the current is increased to 1 A/g from 100 mA/g. In addition, the Couloumbic efficiency at 1 A/g after 500 charge/discharge cycles for potential cycling from 0.5–3.0 V versus Li/Li^+ is 99.9%.

Because of the unique core-shell nanocable structure of the a-TiO_2/CNT nanocomposites, freestanding electrodes could be fabricated by a vacuum filtration process.[72] These freestanding electrodes do not need an organic binder or a current collector. The absence of organic binder and current collector can significantly reduce the "dead" mass and volume compared with conventional electrodes. Most previous studies of freestanding electrodes can only achieve satisfactory performance with a very low active mass loading of at most ~1 mg/cm^2.[73–75] This mass loading is much lower than the mass loading used in real batteries of 5–10 mg/cm^2.

In this work, the TiO_2 mass loading of the freestanding electrodes was 5 mg/cm^2. These electrodes were prepared using the a-TiO_2/CNT nanocomposite with 10% uncoated CNT additive by mass. The

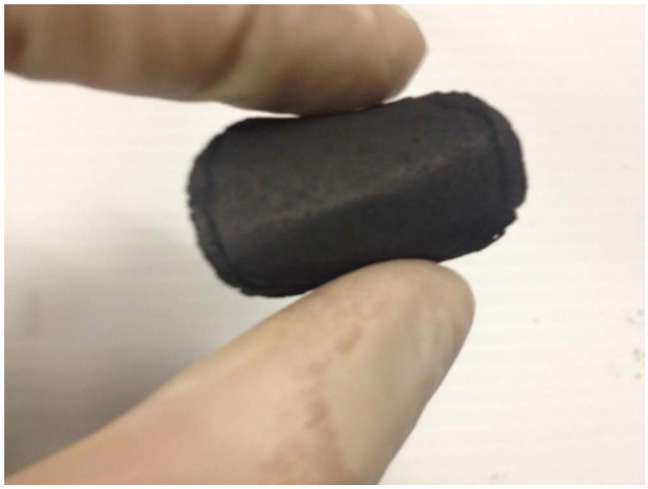

Figure 14. Picture of freestanding TiO_2/CNT paper.

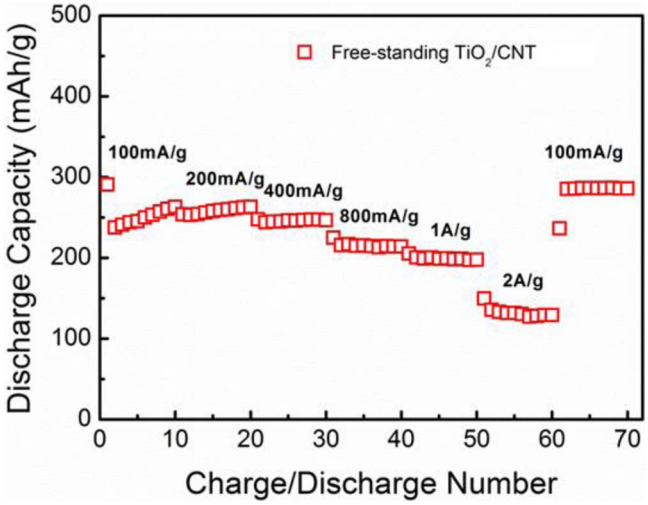

Figure 15. Rate performance of TiO_2/CNT paper fabricated using 100 TiO_2 ALD cycles using a voltage window of 1.0–3.0 V versus Li/Li^+. This sample had a mass loading of 5 mg/cm^2.

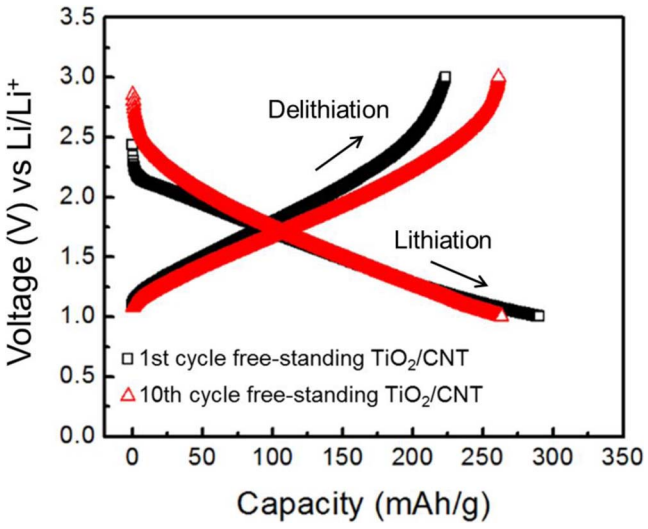

Figure 16. Voltage versus capacity during lithiation and delithiation for the 1st and 10th charge/discharge cycles at 100 mA/g shown in Figure 15.

resulting freestanding electrodes had a thickness of ~130 μm. These freestanding electrodes showed excellent flexibility and mechanical strength. A picture of one of the freestanding electrodes is shown in Figure 14. The electrode was circular and is being bent in the picture in Figure 14.

The discharge capacity for the freestanding electrode at different discharge rates in the voltage range of 1.0–3.0 V versus Li/Li^+ is shown in Figure 15. Figure 16 displays the voltage versus capacity during lithiation and delithiation for the 1st and 10th charge/discharge cycles at 100 mA/g shown in Figure 15. These electrochemical measurements demonstrate that the freestanding TiO_2/CNT paper exhibited a capacity of ~290 mAh/g at 100 mA/g. This capacity at 100 mA/g is higher than the capacity at 100 mA/g in Figure 8. This increased capacity is attributed to the more porous structure of the freestanding electrode. A capacity of 200 mAh/g was still achieved when the current density was increased to 1 A/g. These results are consistent with a capacity retention of ~67% compared with the results at 100 mA/g. This excellent capacity retention at high discharge rates again argues for substantial interfacial charge storage for the TiO_2/CNT nanocomposite. Interfacial charge storage should not be significantly dependent on the discharge rate.

Conclusions

High rate and high power anode materials for lithium ion batteries were fabricated by depositing a-TiO_2 ALD films onto the surface of hydroxyl (–OH) terminated CNT samples. The electrochemical characteristics of TiO_2 ALD films were then determined using cyclic voltammetry and galvanostatic charge/discharge curves. The relatively low electrical conductivity and ionic diffusivity of TiO_2 did not limit these measurements because the TiO_2 ALD films were ultrathin. Using a voltage window of 1.0–3.0V versus Li/Li^+, the specific capacities of the a-TiO_2/CNT nanocomposites at 100 mA/g were 220 mAh/g and 240 mAh/g after 50 and 100 TiO_2 ALD cycles, respectively. 88% of capacity was preserved when the a-TiO_2/CNT nanocomposite after 100 TiO_2 ALD cycles was cycled at 1 A/g. When the current density was further increased to 10 A/g, a capacity of 120 mAh/g was maintained for at least 1000 cycles. CNTs coated with 100 TiO_2 ALD cycles also displayed a high Coulombic efficiency of 83% during the first charge/discharge cycle.

Using an extended voltage window of 0.5–3.0 V versus Li/Li^+, the a-TiO_2/CNT nanocomposites coated with 50 and 100 TiO_2 ALD cycles exhibited discharge capacities at 100 mA/g of 275 mAh/g and 312 mAh/g, respectively. These capacities for the a-TiO_2/CNT nanocomposites are higher than the bulk theoretical values. The extra capacity is attributed to additional interfacial charge storage resulting from the high surface area of the a-TiO_2/CNT nanocomposite. The "box-like" appearance of the current density versus potential was also consistent with capacitive interfacial charge storage. In addition, freestanding TiO_2-CNT electrodes were fabricated with a high TiO_2 mass loadings of ~5 mg/cm^2. These freestanding electrodes also displayed excellent capacity and rate capability. These results illustrate that TiO_2 ALD on high surface area conducting CNT substrates can be employed to form high power and high capacity electrode materials for LIBs.

Acknowledgments

The work at the University of Colorado was supported by the Defense Advanced Research Project Agency (DARPA). The work at Rensselaer Polytechnic Institute was supported by the National Science Foundation (DMR-1151028). Ming Xie and Xiang Sun contributed equally to this work.

References

1. J. M. Tarascon and M. Armand, *Nature*, **414**, 359 (2001).
2. M. S. Whittingham, *Chem. Rev.*, **104**, 4271 (2004).

3. P. G. Bruce, B. Scrosati, and J.-M. Tarascon, *Angew. Chem. Int. Edit.*, **47**, 2930 (2008).
4. G. Jeong, Y.-U. Kim, H. Kim, Y.-J. Kim, and H.-J. Sohn, *Energy Environ. Sci.*, **4**, 1986 (2011).
5. D. Deng, M. G. Kim, J. Y. Lee, and J. Cho, *Energy Environ. Sci.*, **2**, 818 (2009).
6. Z. G. Yang, D. Choi, S. Kerisit, K. M. Rosso, D. H. Wang, J. Zhang, G. Graff, and J. Liu, *J. Power Sources*, **192**, 588 (2009).
7. G. N. Zhu, Y. G. Wang, and Y. Y. Xia, *Energy Environ. Sci.*, **5**, 6652 (2012).
8. Z. Chen, I. Belharouak, Y. K. Sun, and K. Amine, *Adv. Funct. Mater.*, **23**, 959 (2013).
9. J. Y. Shin, D. Samuelis, and J. Maier, *Adv. Funct. Mater.*, **21**, 3464 (2011).
10. J. H. Liu, J. S. Chen, X. F. Wei, X. W. Lou, and X. W. Liu, *Adv. Mater.*, **23**, 998 (2011).
11. N. Li, G. Liu, C. Zhen, F. Li, L. L. Zhang, and H. M. Cheng, *Adv. Funct. Mater.*, **21**, 1717 (2011).
12. H. Han, T. Song, J. Y. Bae, L. F. Nazar, H. Kim, and U. Paik, *Energy Environ. Sci.*, **4**, 4532 (2011).
13. J. Y. Shin, J. H. Joo, D. Samuelis, and J. Maier, *Chem. Mater.*, **24**, 543 (2012).
14. D. D. Cai, P. C. Lian, X. F. Zhu, S. Z. Liang, W. S. Yang, and H. H. Wang, *Electrochim. Acta*, **74**, 65 (2012).
15. S. B. Yang, X. L. Feng, and K. Mullen, *Adv. Mater.*, **23**, 3575 (2011).
16. S. H. Liu, H. P. Jia, L. Han, J. L. Wang, P. F. Gao, D. D. Xu, J. Yang, and S. N. Che, *Adv. Mater.*, **24**, 3201 (2012).
17. G. F. Ortiz, I. Hanzu, T. Djenizian, P. Lavela, J. L. Tirado, and P. Knauth, *Chem. Mater.*, **21**, 63 (2008).
18. M. Wagemaker, G. J. Kearley, A. A. van Well, H. Mutka, and F. M. Mulder, *J. Am. Chem. Soc.*, **125**, 840 (2002).
19. H. Lindstrom, S. Sodergren, A. Solbrand, H. Rensmo, J. Hjelm, A. Hagfeldt, and S. E. Lindquist, *J. Phys. Chem. B*, **101**, 7710 (1997).
20. H. Liu, Z. Bi, X.-G. Sun, R. R. Unocic, M. P. Paranthaman, S. Dai, and G. M. Brown, *Adv. Mater.*, **23**, 3450 (2011).
21. G. Armstrong, A. R. Armstrong, J. Canales, and P. G. Bruce, *Electrochem. Solid State Lett.*, **9**, A139 (2006).
22. A. R. Armstrong, G. Armstrong, J. Canales, and P. G. Bruce, *Angew. Chem. Int. Edit.*, **43**, 2286 (2004).
23. J. Wang, J. Polleux, J. Lim, and B. Dunn, *J. Phys. Chem. C*, **111**, 14925 (2007).
24. S. Yoon, B. H. Ka, C. Lee, M. Park, and S. M. Oh, *Electrochem Solid St*, **12**, A28 (2009).
25. Z. X. Yang, G. D. Du, Z. P. Guo, X. B. Yu, Z. X. Chen, T. L. Guo, and H. K. Liu, *J Mater Chem*, **21**, 8591 (2011).
26. D. H. Wang, D. W. Choi, J. Li, Z. G. Yang, Z. M. Nie, R. Kou, D. H. Hu, C. M. Wang, L. V. Saraf, J. G. Zhang, I. A. Aksay, and J. Liu, *ACS Nano*, **3**, 907 (2009).
27. L. F. Shen, X. G. Zhang, H. S. Li, C. Z. Yuan, and G. Z. Cao, *J. Phys. Chem. Lett.*, **2**, 3096 (2011).
28. S. M. George, *Chem. Rev.*, **110**, 111 (2010).
29. J. W. Elam, D. Routkevitch, P. P. Mardilovich, and S. M. George, *Chem. Mater.*, **15**, 3507 (2003).
30. R. G. Gordon, D. Hausmann, E. Kim, and J. Shepard, *Chem. Vap. Deposition*, **9**, 73 (2003).
31. Y. S. Jung, A. S. Cavanagh, L. A. Riley, S. H. Kang, A. C. Dillon, M. D. Groner, S. M. George, and S. H. Lee, *Adv. Mater.*, **22**, 2172 (2010).
32. I. Lahiri, S.-M. Oh, J. Y. Hwang, C. Kang, M. Choi, H. Jeon, R. Banerjee, Y.-K. Sun, and W. Choi, *J Mater Chem*, **21**, 13621 (2011).
33. C. M. Ban, M. Xie, X. Sun, J. J. Travis, G. K. Wang, H. T. Sun, A. C. Dillon, J. Lian, and S. M. George, *Nanotechnology*, **24**, 424002 (2013).
34. X. Y. Chen, H. L. Zhu, Y. C. Chen, Y. Y. Shang, A. Y. Cao, L. B. Hu, and G. W. Rubloff, *Acs Nano*, **6**, 7948 (2012).
35. X. F. Li, X. B. Meng, J. Liu, D. S. Geng, Y. Zhang, M. N. Banis, Y. L. Li, J. L. Yang, R. Y. Li, X. L. Sun, M. Cai, and M. W. Verbrugge, *Adv. Funct. Mater.*, **22**, 1647 (2012).
36. S. Boukhalfa, K. Evanoff, and G. Yushin, *Energy Environ. Sci.*, **5**, 6872 (2012).
37. X. Sun, M. Xie, J. J. Travis, G. K. Wang, H. T. Sun, J. Lian, and S. M. George, *J. Phys. Chem. C*, **117**, 22497 (2013).
38. X. Sun, M. Xie, G. K. Wang, H. T. Sun, A. S. Cavanagh, J. J. Travis, S. M. George, and J. Lian, *J. Electrochem. Soc.*, **159**, A364 (2012).
39. S. K. Cheah, E. Perre, M. Rooth, M. Fondell, A. Harsta, L. Nyholm, M. Boman, T. Gustafsson, J. Lu, P. Simon, and K. Edstrom, *Nano Lett.*, **9**, 3230 (2009).
40. W. Wang, M. Tian, A. Abdulagatov, S. M. George, Y.-C. Lee, and R. Yang, *Nano Lett.*, **12**, 655 (2012).
41. K. Gerasopoulos, E. Pomerantseva, M. McCarthy, A. Brown, C. Wang, J. Culver, and R. Ghodssi, *ACS Nano*, **6**, 6422 (2012).
42. E. Eustache, P. Tilmant, L. Morgenroth, P. Roussel, G. Patriarche, D. Troadec, N. Rolland, T. Brousse, and C. Lethien, *Adv. Energy Mater.*, **4**, 1301612 (2014).
43. H. T. Fang, M. Liu, D. W. Wang, T. Sun, D. S. Guan, F. Li, J. G. Zhou, T. K. Sham, and H. M. Cheng, *Nanotechnology*, **20**, 225701 (2009).
44. W. J. H. Borghols, D. Lutzenkirchen-Hecht, U. Haake, W. Chan, U. Lafont, E. M. Kelder, E. R. H. van Eck, A. P. M. Kentgens, F. M. Mulder, and M. Wagemaker, *J. Electrochem. Soc.*, **157**, A582 (2010).
45. Z. Bi, M. P. Paranthaman, P. A. Menchhofer, R. R. Dehoff, C. A. Bridges, M. Chi, B. Guo, X.-G. Sun, and S. Dai, *J. Power Sources*, **222**, 461 (2013).
46. Y. M. Lin, P. R. Abel, D. W. Flaherty, J. Wu, K. J. Stevenson, A. Heller, and C. B. Mullins, *J. Phys. Chem. C*, **115**, 2585 (2011).
47. H. Xiong, H. Yildirim, E. V. Shevchenko, V. B. Prakapenka, B. Koo, M. D. Slater, M. Balasubramanian, S. K. R. S. Sankaranarayanan, J. P. Greeley, S. Tepavcevic, N. M. Dimitrijevic, P. Podsiadlo, C. S. Johnson, and T. Rajh, *J. Phys. Chem. C*, **116**, 3181 (2012).
48. A. S. Cavanagh, C. A. Wilson, A. W. Weimer, and S. M. George, *Nanotechnology*, **20**, 255602 (2009).
49. J. Aarik, A. Aidla, T. Uustare, and V. Sammelselg, *J. Cryst. Growth*, **148**, 268 (1995).
50. J. A. McCormick, B. L. Cloutier, A. W. Weimer, and S. M. George, *J. Vac. Sci. Technol. A*, **25**, 67 (2007).
51. J. A. McCormick, K. P. Rice, D. F. Paul, A. W. Weimer, and S. M. George, *Chem. Vap. Deposition*, **13**, 491 (2007).
52. M. Ritala, M. Leskela, E. Nykanen, P. Soininen, and L. Niinisto, *Thin Solid Films*, **225**, 288 (1993).
53. W. Z. Li, C. H. Liang, W. J. Zhou, J. S. Qiu, Z. H. Zhou, G. Q. Sun, and Q. Xin, *J. Phys. Chem. B*, **107**, 6292 (2003).
54. C. H. Liang, L. Ding, C. Li, M. Pang, D. S. Su, W. H. Li, and Y. M. Wang, *Energy & Environ. Sci.*, **3**, 1121 (2010).
55. X. B. Yan, B. K. Tay, and Y. Yang, *J. Phys. Chem. B*, **110**, 25844 (2006).
56. G. M. An, W. H. Ma, Z. Y. Sun, Z. M. Liu, B. X. Han, S. D. Miao, Z. J. Miao, and K. L. Ding, *Carbon*, **45**, 1795 (2007).
57. B. S. Huang, H. H. Tseng, and M. Y. Wey, *J. Ceram. Soc. Jp.*, **117**, 753 (2009).
58. B. J. Landi, M. J. Ganter, C. D. Cress, R. A. DiLeo, and R. P. Raffaelle, *Energy Environ. Sci.*, **2**, 638 (2009).
59. M. Pumera, *Energy Environ. Sci.*, **4**, 668 (2011).
60. M. Winter, *Z. Phys. Chem.*, **223**, 1395 (2009).
61. Z.-S. Wu, W. Ren, L. Xu, F. Li, and H.-M. Cheng, *ACS Nano*, **5**, 5463 (2011).
62. Z. X. Shu, R. S. Mcmillan, and J. J. Murray, *J. Electrochem. Soc.*, **140**, 922 (1993).
63. T. Zheng, Y. H. Liu, E. W. Fuller, S. Tseng, U. Vonsacken, and J. R. Dahn, *J. Electrochem. Soc.*, **142**, 2581 (1995).
64. F. F. Cao, Y. G. Guo, S. F. Zheng, X. L. Wu, L. Y. Jiang, R. R. Bi, L. J. Wan, and J. Maier, *Chem. Mater.*, **22**, 1908 (2010).
65. J. Liu, X. F. Li, M. Cai, R. Y. Li, and X. L. Sun, *Electrochim. Acta*, **93**, 195 (2013).
66. T. Abe, S. Yamate, Y. Iriyama, M. Inaba, Z. Ogumi, and T. Fukutsuka, *Mol. Cryst. Liq. Cryst.*, **388**, 555 (2002).
67. P. Balaya, A. J. Bhattacharyya, J. Jamnik, Y. F. Zhukovskii, E. A. Kotomin, and J. Maier, *J. Power Sources*, **159**, 171 (2006).
68. J. Jamnik and J. Maier, *Phys. Chem. Chem. Phys.*, **5**, 5215 (2003).
69. Y. F. Zhukovskii, P. Balaya, E. A. Kotomin, and J. Maier, *Phys. Rev. Lett.*, **96**, 058302 (2006).
70. B. E. Conway, *J. Electrochem. Soc.*, **138**, 1539 (1991).
71. M. Toupin, T. Brousse, and D. Belanger, *Chem. Mater.*, **14**, 3946 (2002).
72. X. Jia, Z. Chen, X. Cui, Y. Peng, X. Wang, G. Wang, F. Wei, and Y. Lu, *ACS Nano*, **6**, 9911 (2012).
73. M. N. Hyder, B. M. Gallant, N. J. Shah, Y. Shao-Horn, and P. T. Hammond, *Nano Lett.*, **13**, 4610 (2013).
74. S. Liu, Z. Wang, C. Yu, H. B. Wu, G. Wang, Q. Dong, J. Qiu, A. Eychmüller, and X. W. Lou, *Adv. Mater.*, **25**, 3462 (2013).
75. X. Wang, Y. Yan, B. Hao, and G. Chen, *ACS Appl. Mater. Interfaces*, **5**, 3631 (2013).